Letter

Quantum Dynamical Approach to Predicting the Optical Pumping Threshold for Lasing in Organic Materials

Bin Zhang and Zhigang Shuai*

Cite This: *J. Phys. Chem. Lett.* 2023, 14, 8590−8598
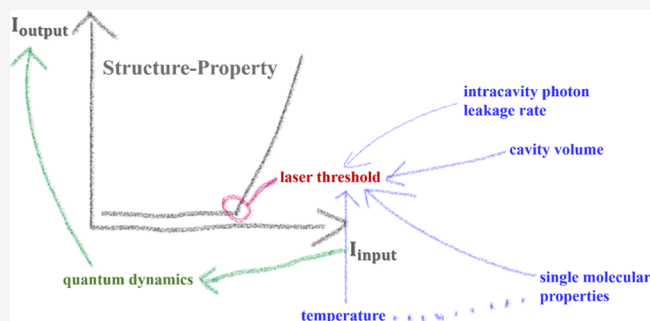
Read Online

ACCESS | Metrics & More | Article Recommendations | Supporting Information

ABSTRACT: The quantum dynamic (QD) study of organic lasing (OL) is a challenging issue in organic optoelectronics. Previously, the phenomenological method has achieved success in describing experimental observation. However, it cannot directly bridge the laser threshold (LT) with microscopic parameters, which is the advantage of the QD method. In this paper, we propose a microscopic OL model and apply time-dependent wave packet diffusion to reveal the microscopic QD process of optically pumped lasing. LT is obtained from the onset of output as a function of optical input pumping. We predict that the LT has an optimal value as a function of the cavity volume and depends linearly on the intracavity photon leakage rate. The calculated structure−property relationships between molecular parameters and the LT are in qualitative agreement with the experimental results, confirming the reliability of our approach. This work is beneficial for understanding the OL mechanism and optimizing the design of organic laser materials.

The development of organic solid-state lasers (OSSLs) has been greatly promoted over the past few years, due to their wide wavelength range and low-cost fabrication.[1,6,10,15,19,20] As we know, organic lasers have been developed for 20 years,[30] including the optically pumped laser,[19,20] the electrically pumped laser,[27,34] and the polariton laser.[14,32,38] At present, the most mature research of OSSLs is that involving the optically pumped laser. Because of the optimization of the gain medium, the high-Q cavity feedback structure, and the excellent optical excitation system, the performance of the optically pumped laser has been remarkably improved,[30] and the high-Q optical cavity has become a new way to manipulate the molecular photophysical properties by light−matter coupling. Because organic molecular materials have achieved great success in diverse fields,[6,47] the theoretical design of organic laser molecules has attracted a great deal of attention. In the previous work by our group,[34,41] computational selection strategies for optically pumped and electrically pumped organic laser molecules have been proposed. Compared to the theoretical design of laser molecules, there is still little research on the mechanism of organic lasers, particularly the dynamic process of intracavity photons.

The formation of a laser requires an optical gain to compensate for the photon leakage in the optical cavity.[6,19,30] The laser threshold is a crucial parameter for describing the organic laser performance. The laser threshold is a particular pump power. When the pump power is larger than the laser threshold, the output power not only increases significantly but also increases linearly with the input power. Above the laser threshold, the larger output power for a given input power corresponds to a larger slope. It is easy to understand that the lifetime of the exciton and photon in the cavity is very important for the laser threshold, and increasing the lifetime of the exciton and photon can reduce the laser threshold. Excellent laser performance usually corresponds to a low laser threshold. On the basis of phenomenological theory, Adachi's group has studied the influence of different excitonic losses and photon leakage on the organic laser threshold of organic lasers under optical and electrical excitations.[42,43] However, the phenomenological method cannot directly connect the laser threshold and cavity parameters and molecular electronic structure parameters. In this paper, we directly relate the input variable and the output variable of organic lasers to obtain the lasing threshold based on the quantum dynamical method and then investigate the structure−property relationships between the laser threshold and the cavity parameters (including intracavity photon leakage rate and cavity volume) and molecular electronic structure parameters (including the energy of the molecular excited state, the transition dipole,

and the organization energy). Finally, we obtain the physical picture of organic lasers and the related structure−property relationships. The outline of this paper is as follows. First, we extend the time-dependent wave packet diffusion (TDWPD)[9,12,17,39] method, including the light−matter interaction for describing the organic laser in a dissipative cavity. Then, we combine the extended TDWPD coupled with properly electronic structure calculations of 4,4′-bis[(N-carbazole)styryl]biphenyl (BSBCz)[23] to investigate the structure−property relationship among the intracavity photon leakage rate, cavity volume, single-molecule electronic structure properties, and laser threshold. Finally, we investigate the influence of the temperature and the external field duration on the laser threshold. The proposed formalism and the structure−property relationship are beneficial to understanding the mechanism of an organic laser and optimizing the design of organic laser materials.

In this paper, we study the system, which is N identical molecules inside a dissipative optical cavity. The interaction strength between the ith molecule and intracavity photon $\hbar g_i$ can be written as[21,35]

$$\hbar g_i = |\vec{\mu}_{eg}| \sqrt{\frac{\hbar \omega_P}{2\varepsilon_0 \varepsilon_\infty V}} \cos \theta_i \tag{1}$$

where $\vec{\mu}_{eg}$ is the transition dipole moment (TDM) of the S_1 state, ω_P is the frequency of the intracavity photon, ε_0 is the vacuum permittivity, ε_∞ is the optical dielectric constant of the matrix inside the cavity, V is the cavity mode volume, and θ_i is the angle between the TDM of the ith S_1 state and the intracavity photon. Within the random orientation model (Supporting Information), disorder molecules are independent of each other. Therefore, the lasing process of each molecule can be independently studied, and we assume that each molecule only effectively couples one intracavity photon; they compose a subsystem that is also independent of each other. Therefore, we can use the quantum dynamics method to calculate the dynamical properties inside the subsystem, including one molecule and one photon, and then obtain the properties of the total intracavity system. The effective coupling $\hbar \bar{g}$ can be expressed as

$$\hbar \bar{g} = \frac{1}{\sqrt{3}} |\vec{\mu}_{eg}| \sqrt{\frac{\hbar \omega_P}{2\varepsilon_0 \varepsilon_\infty V}} \tag{2}$$

In the following text, we use cavity length L_{cavity} to replace cavity volume $V = L_{cavity}^3$ and use V_{eP} to replace effective exciton−photon coupling $\hbar \bar{g}$. It is noteworthy that the random orientation model may not be valid for a very small cavity. In the case of a very small cavity, the exciton−photon coupling strength is dependent on the molecular position.[29,36] Meanwhile, the property of intracavity photons is also dependent on the molecular position for a small cavity.[29,36] We will develop our theoretical model for the small cavity. To describe the organic lasing dynamics in a dissipative cavity, the total Hamiltonian can be expressed as

$$\hat{H}(t) = \hat{H}_e(t) + \hat{H}_{photon} + \hat{H}_{phonon} + \hat{H}_{loss} + \hat{H}_{e\text{-}photon}$$
$$+ \hat{H}_{e\text{-}phonon} + \hat{H}_{photon\text{-}loss}$$
$$= \hat{H}_E(t) + \hat{H}_{E\text{-}bath} + \hat{H}_{bath} \tag{3}$$

where $\hat{H}_e(t)$, $\hat{H}_{phonon}$, $\hat{H}_{e\text{-}phonon}$, $\hat{H}_{photon}$, $\hat{H}_{e\text{-}photon}$, $\hat{H}_{loss}$, and $\hat{H}_{photon\text{-}loss}$ denote the Hamiltonian for the exciton, the vibrations (or phonon), the exciton−phonon couplings, the intracavity photon, the light−matter interaction, the outside cavity bath, and the intracavity photon−outside cavity bath coupling, respectively, $\hat{H}_E(t) = \hat{H}_e(t) + \hat{H}_{photon} + \hat{H}_{e\text{-}photon}$, $\hat{H}_{E\text{-}bath} = \hat{H}_{e\text{-}phonon} + \hat{H}_{photon\text{-}loss}$, and $\hat{H}_{bath} = \hat{H}_{phonon} + \hat{H}_{loss}$. The Hamiltonian inside the intracavity subsystem that includes one molecule and one photon can be written as

$$\begin{cases} \hat{H}_e(t) = \varepsilon_g|g\rangle\langle g| + \varepsilon_e|e\rangle\langle e| - \vec{\hat{\mu}}_{eg} \cdot \vec{E}_{pump}(t) \\[6pt] \hat{H}_{photon} = \hbar \omega_P \left(\hat{c}_P^\dagger \hat{c}_P + \frac{1}{2} \right) \\[6pt] \hat{H}_{phonon} = \sum_{j=1}^{N_{ph}^e} \hbar \omega_j^e \left(\hat{a}_{ej}^\dagger \hat{a}_{ej} + \frac{1}{2} \right) \\[6pt] \hat{H}_{loss} = \sum_{j=1}^{N_b^P} \hbar \omega_j^P \left(\hat{b}_{Pj}^\dagger \hat{b}_{Pj} + \frac{1}{2} \right) \\[6pt] \hat{H}_{E\text{-}photon} = V_{eP}|e\rangle\langle g|\hat{c}_P + \text{h.c.} \\[6pt] \hat{H}_{E\text{-}phonon} = \sum_{j=1}^{N_{ph}^e} C_j^e (\hat{a}_{ej}^\dagger + \hat{a}_{ej})|e\rangle\langle e| \\[6pt] \hat{H}_{photon\text{-}loss} = \sum_{j=1}^{N_b^P} C_j^P (\hat{b}_{Pj}^\dagger + \hat{b}_{Pj})(\hat{c}_P^\dagger + \hat{c}_P) \end{cases} \tag{4}$$

where ε_g, ω_P, and ε_e are the energies of ground state $|g\rangle$, photonic state $\hat{c}_P^\dagger|g\rangle$, and localized singlet excited state $|e\rangle$, respectively. In this work, the phonon and outside cavity bath are identified by a collection of harmonic oscillators. C_j^e is the mode-specific electron-vibrational coupling strength, and it is determined by the spectral density $J_e(\omega) = \pi \sum_j C_j^{e2} \delta(\omega - \omega_j^e)$. C_j^P represents the intracavity photon−outside cavity bath coupling strength, and it is determined by the spectral density $J_P(\omega) = \pi \sum_j C_j^{P2} \delta(\omega - \omega_j^P)$. Here, we set $\vec{\mu}_{eg} \cdot \vec{E}_{pump}(t) \approx |\mu_{eg}|E_{pump}(t)/\sqrt{3}$, which is also the result based on the random orientation approximation. External field $E_{pump}(t)$ is $E_{pump}(t) = \frac{E_0}{\sqrt{2\pi}\sigma} e^{-t^2/2\sigma^2} \cos(\omega_{pump} t)$, where σ, E_0, and ω_{pump} are the field duration, field strength, and field frequency, respectively. Hereafter, we use μ_{eg} to replace $|\mu_{eg}|$. For resonance excitation, we set $\hbar \omega_{pump}$ equal to ε_e. The formulas and the parameter setting of their spectral density will be described in detail below. In the quantum dynamic simulations, we adopt the TDWPD method[9,12,17] because it can be easily applied to large complex systems and extended to incorporate the strong light−matter coupling. Recently, the TDWPD method has been extended to include the light−matter interaction and used to successfully investigate the effect of the optical microcavity on the singlet fission dynamics in organic systems.[39] The results of previous research have shown that the TDWPD method is indeed suitable for studying the dynamic properties of complex molecular systems

incorporating the light−matter interaction. The TDWPD method is one of the stochastic Schrödinger equations (SSEs) in which the molecular vibrational motions are described by random fluctuations on each electronic state, and the dynamical equation can be written as

$$i\frac{\partial}{\partial t}|\Psi(t)\rangle = \left[\hat{H}_E(t) + \hat{F}(t) - i\hat{L}\int_0^t d\tau \alpha_{T=0}(\tau)\right.$$
$$\left. e^{i\int_0^\tau \hat{H}_E(\tau')\,d\tau'}\hat{L}^\dagger e^{-i\int_0^\tau \hat{H}_E(\tau')\,d\tau'}\right]|\Psi(t)\rangle \tag{5}$$

where $\hat{H}_E(t)$ is the intracavity system Hamiltonian, $\hat{F}(t)$ is the stochastic force operator $\hat{F}(t) = \sum_{n,m} F_{nm}(t)|n\rangle\langle m|$, $\alpha_{T=0}(t)$ is the zero-temperature correlation function $\alpha_{T=0}(t) = \sum_j C_j^{n2} e^{-i\omega_j^n t}$, and $\hat{L}$ is the projection operator. The states $|n(m)\rangle$ include ground state $|g\rangle$, excited state $|e\rangle$, and intracavity photon state $|P\rangle$, and $\hat{L} = |e\rangle\langle e|, |g\rangle\langle P|$, and $|P\rangle\langle g|$ correspond to excited state $|e\rangle$, ground state $|g\rangle$, and intracavity photon state $|P\rangle$, respectively. The complete relation is

$$1 = |e\rangle\langle e| + |g\rangle\langle g| + |P\rangle\langle P| \tag{6}$$

In numerical calculations, wave function $|\Psi(t)\rangle$ is written as

$$|\Psi(t)\rangle = A_e(t)|e\rangle + A_g(t)|g\rangle + A_P(t)|P\rangle \tag{7}$$

The differential equations of the time-dependent coefficients $\{A_j(t)\}$ (j = g, e, or P) are

$$\begin{cases} i\frac{\partial}{\partial t}A_e(t) = [\varepsilon_e + F_e(t)]A_e(t) + V_{eP}A_P(t) \\ \qquad - [\vec{\mu}_{eg}\cdot\vec{E}_{pump}(t)]A_g(t) \\ \qquad - i\sum_k \int_0^t d\tau \alpha_e(\tau)\left\langle e\left|e^{i\int_0^\tau \hat{H}_E(\tau')\,d\tau'}\right|e\right\rangle\left\langle e\left|e^{-i\int_0^\tau \hat{H}_E(\tau')\,d\tau'}\right|\right. \\ \qquad\qquad \left.k\right\rangle A_k(t), \\[1em] i\frac{\partial}{\partial t}A_g(t) = \varepsilon_g A_g(t) + F_g(t)A_P(t) - [\vec{\mu}_{eg}\cdot\vec{E}_{pump}(t)] \\ \qquad A_e(t) \\ \qquad - i\sum_k \int_0^t d\tau \alpha_g(\tau)\left\langle P\left|e^{i\int_0^\tau \hat{H}_E(\tau')\,d\tau'}\right|P\right\rangle \\ \qquad\qquad \left\langle g\left|e^{-i\int_0^\tau \hat{H}_E(\tau')\,d\tau'}\right|k\right\rangle A_k(t), \\[1em] i\frac{\partial}{\partial t}A_P(t) = \hbar\omega_P A_P(t) + V_{eP}A_e(t) + F_P(t)A_g(t) \\ \qquad - i\sum_k \int_0^t d\tau \alpha_P(\tau)\left\langle g\left|e^{i\int_0^\tau \hat{H}_E(\tau')\,d\tau'}\right|g\right\rangle \\ \qquad\qquad \left\langle P\left|e^{-i\int_0^\tau \hat{H}_E(\tau')\,d\tau'}\right|k\right\rangle A_k(t) \end{cases} \tag{8}$$

where $F_{e(P)}(t)$ is the stochastic force, which can be generated by

$$F_{e(P)}(t) = \sum_k \sqrt{\frac{J_{e(P)}(\omega_k)\triangle\omega}{\pi}}\left[\sqrt{A(\omega_k)}\,\cos(\omega_k t + \phi_k)\right.$$
$$\left. + i\sqrt{B(\omega_k)}\,\sin(\omega_k t + \phi_k)\right] \tag{9}$$

where $A(\omega_k) = \coth(\omega_k/2k_B T) + \operatorname{csch}(\omega_k/2k_B T)$ and $B(\omega_k) = \coth(\omega_k/2k_B T) - \operatorname{csch}(\omega_k/2k_B T)$. $\{\phi_k\}$ is a series of random variables that are uniformly distributed in $[0, 2\pi]$. $\alpha_e(t) = \sum_j C_j^{e2} e^{-i\omega_j^e t}$ and $\alpha_P(t) = \sum_j C_j^{P2} e^{-i\omega_j^P t}$ are the zero-temperature correlation function of the exciton−phonon couplings and the intracavity photon−outside cavity bath couplings, respectively. From the TDWPD equation (eq 8), we can obtain the time-dependent coefficients $\{A_j(t)\}$ (j = g, e, or P). The population dynamics can be obtained by the stochastic average of $A_{e(g, or P)}(t)$. For instance, the time evolution of a population on the i (i = e, g, or P)th state is calculated by $P_i(t) = \langle A_i^*(t)A_i(t)\rangle$. The input variable is the intensity of the incident laser pulse (I_{input}), and it can be defined as

$$I_{input} \propto |E_0|^2 \tag{10}$$

where 1.0 au field strength $|E_0|$ corresponds to 3.5094×10^{13} KW/cm^2 input intensity I_{input}.[8,33] Although I_{input} is the input variable, we directly change field strength E_0 in numerical calculations. The output variable is I_{output}, which is the steady-state photon density inside the cavity, and can be defined as

$$I_{output} = \lim_{t\to\infty} P_P(t)c_M N_A \tag{11}$$

where $P_P(t)$ is the population of the photon state inside the intracavity subsystem that includes one molecule and one photon, $c_M = N/V$ is the doping concentration of the molecule, N_A is Avogadro's constant, and $\lim_{t\to\infty} P_P(t)$ is the population of the intracavity photon state when the intracavity system reaches its thermal equilibrium state. For the intracavity system that includes excitons, phonons, and photons, we use different intensities of external fields I_{input} to excite molecules and transfer the population to the intracavity photon state through exciton−intracavity photon coupling. When the steady state is reached, the intracavity photon density is calculated to obtain output variable I_{output}.

Molecular Properties of BSBCz. In this paper, we use BSBCz as a test molecule. In the previous work of our group, BSBCz has not only excellent photopumped laser performance but also excellent electro-pumped laser performance.[34] We use TD-B3LYP/6-31g* to calculate the single-molecule properties of BSBCz with Gaussian16.[22] This theoretically predicted that the energy of the S_1 state is 2.472 eV, and the transition dipole is 6.839 au. On the basis of the knowledge of electronic structure, we compute the rate constants of different physical processes by the TVCF rate formalism.[16,28,37] All rate constant calculations are performed via thermal vibration correlation function (TVCF) method in MOMAP 2021A.[7,26,31] This theoretically predicted that the radiative rate of the S_1 state (k_r) is 6.5×10^8 s^{-1} and the internal conversion rate of the S_1 state (k_{ic}) is 1.5×10^8 s^{-1}, which are consistent with the numerical results in ref 34. The Lorentzian broadening full width at half-maximum of 200 cm^{-1} has been used for the convergence of k_{ic}. Here, we also display the molecular reorganization energy distribution shown in Figure 2. In the following, we determine the intramolecular vibration spectral density based on the reorganization energy distribution. It is noteworthy that we also can employ the effective vibronic mode to effectively
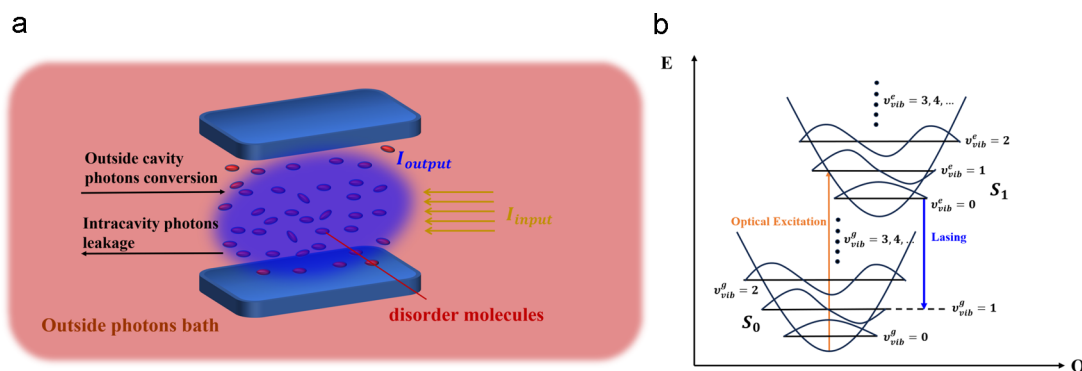
Figure 1. (a) Schematic graph of organic lasers in a dissipative cavity. (b) Molecular four-level energy system, where E is the energy and Q is the vibrational coordinate.

represent all vibrational modes by following a number of previous works.[2−5,11,17,45,46] The schematic depiction for the lasing process is shown in Figure 1 b. Huang−Rhys factor S_{eff}, frequency ω_{eff}, and reorganization energy λ_{eff} of the effective vibronic mode can be calculated as $S_{\text{eff}} = \sum_i S_i$, $\omega_{\text{eff}} = \sum_i \frac{\omega_i S_i}{S_{\text{eff}}}$, and $\lambda_{\text{eff}} = \omega_{\text{eff}} S_{\text{eff}}$, respectively, where Huang−Rhys factors $\{S_i\}$, frequencies $\{\omega_i\}$, and reorganization energies $\{\lambda_i\}$ are the parameters of all vibronic modes.

Quantum Dynamics Results of Organic Lasers. Next, we calculate the laser dynamics and the structure−property relationship among the intracavity photon−outside cavity bath coupling strength, cavity size, single-molecule electronic structure properties, and laser threshold. Before the numerical calculations, we summarize the extended TDWPD method and the calculation method of the main physical quantities involved in this Letter. In this paper, we study the system that is N identical molecules inside a dissipative optical cavity. On the basis of the random orientation approximation, the disorder molecules inside the cavity are independent of each other. The lasing process of each molecule can be independently studied. We assume that each molecule only effectively couples one intracavity photon, and they compose a subsystem that is also independent. Therefore, we can use the quantum dynamics method to calculate the dynamical properties inside the subsystem that includes one molecule and one photon and then obtain the properties of the total intracavity system. In the quantum dynamic simulations, we adopt the TDWPD method[9,12,17] because it can be easily applied to large systems and extended to incorporate the strong light−matter coupling. Recently, the TDWPD method has been extended to include the light−matter interaction and used to successfully investigate the effect of the optical microcavity on the singlet fission dynamics in an organic system.[39] The results of previous research have shown that the TDWPD method is indeed suitable for studying the dynamic properties of complex molecular systems incorporating the light−matter interaction. The TDWPD method is one of the stochastic Schrödinger equations (SSEs) in which the molecular vibrational motions are described by random fluctuations on each electronic state. From the TDWPD equation (eq 8), we can obtain the time-dependent coefficients $\{A_j(t)\}$ (j = g, e, or P). The population dynamics is thus obtained by the stochastic average of $A_{\text{e(g, or P)}}(t)$. For example, the time evolution of the population on the i (i = e, g, or P)th state is calculated by $P_i(t) = \langle A_i^*(t) A_i(t) \rangle$. Input variable I_{input} [$I_{\text{input}} \propto |E_0|^2$ (see eq 10)] is the intensity of incident laser pulse $E_{\text{pump}}(t)$, and we change the

intensity of the incident laser pulse by changing the value of field strength E_0 in the numerical calculations. Output variable I_{output} [$I_{\text{output}} = \lim_{t\to\infty} P_P(t) c_M N_A$ (see eq 11)] is the steady-state photon density inside the cavity, and doping concentration c_M is 0.15×10^{-3} M.[23] Next, we can obtain laser threshold I_{thred} and field strength threshold E_{thred} through the inflection point of the I_{output}−I_{input} curve. Following the preceding calculation process, we can obtain the structure−property relationships between laser threshold I_{thred} and cavity parameters and molecular electronic structure parameters.

For our microscopic model, the coupling between the intracavity photons and the bath is actually the coupling between the intracavity photons and the continuous photon environment outside the cavity. It leads to the intracavity photons leaking into the photon environment outside the cavity, manifested as the quenching of the intracavity photons. Similarly, if there are no intracavity photons and the intracavity photon−bath coupling is relatively large, the photons outside the cavity will also penetrate the cavity (at the initial time, the initial state of the photon environment is a thermal equilibrium distribution). Therefore, there will be a small amount of population of the intracavity photon state without external field $E_{\text{pump}}(t)$ excitation. The schematic graph is shown in Figure 1. The population dynamics of the intracavity system at exciton−photon coupling V_{eP} also confirms the physical picture, shown in Figures S5 and S6. Exciton−phonon coupling C_{ej} is described by the spectral density with broadened stick spectra of pseudolocal phonon modes,[13,24] $J_e(\omega) = \frac{1}{\pi} \sum_k \frac{\lambda_k \omega \gamma}{(\omega - \omega_k)^2 + \gamma^2}$, which includes information about all of the vibrational modes for studying the dynamical properties of the realistic molecular system with a uniform broadening factor of γ = 40.0 meV to smoothly generate fluctuation energies.[25] Reorganization energy λ_k is calculated via the vibrational modes of the monomer, as shown in Figure 2. Coupling strength C_j^P is that between intracavity photons, and we use the Debye spectral density $J_P(\omega) = \frac{2\lambda_P \omega \omega_P^c}{\omega^2 + \omega_P^{c2}}$ to describe the bath, which is consistent with David Reichman's recent work.[44] We set the characteristic frequency of the photon environment outside the cavity ω_P^c to 1450 cm^{-1}. According to spectral density $J_P(\omega)$, we can calculate the corresponding leakage rate of the intracavity photon $\Gamma_P = \frac{1}{\tau_P} = \frac{2J_P(\omega_P)}{1 - e^{-\beta\omega_P}}$, where τ_c is the intracavity photon lifetime and $\beta = \frac{1}{k_B T}$ with the Boltzmann constant k_B and temperature T (300 K), and then obtain the
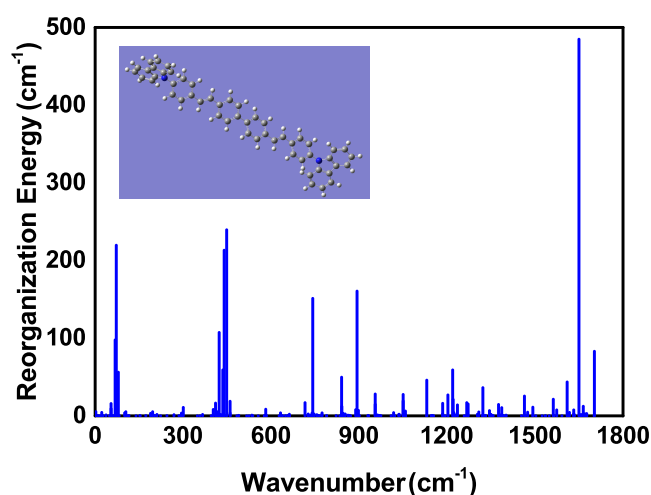
Figure 2. Reorganization energy distribution of BSBCz. The inset shows the chemical structure of BSBCz.

quality of the cavity (Q value) $Q = \frac{1}{2}\frac{\omega_P}{\Gamma_P}$.[42,43] The relevant results are listed in Table 1. The exciton–photon coupling strength is shown in Table 3. In this paper, we set the resonance between the external field energy and the S_1 state of the molecule. From Figure 7, we can see that duration σ is almost independent of the laser threshold. Without a loss of generality, we set σ to be 30.0 fs later.

First, we calculated the structure–property relationship among intracavity photon–outside cavity bath coupling strength λ_P, cavity length L_{cavity}, and laser threshold I_{thred}. The calculated results are shown in Figure 3. Figure 3a shows the structure–property relationship among intracavity photon–outside cavity bath coupling strength λ_P, cavity length L_{cavity}, and laser threshold I_{thred}, while Figure 3b shows the population dynamics of the photon state. Without a loss of generality, we see that the quality of this order of magnitude is often used for research in experiments; λ_P is 0.5 meV. From the results of the calculation, one can see that laser threshold I_{thred} first decreases and then increases as L_{cavity} increases, which can be understood from a physical perspective. The external field will destroy the equilibrium state of the system and bring it to a new stable state. Only when the intensity of external field $E_{pump}(t)$ is sufficient to break the equilibrium state of the system will the lasing phenomenon occur, which manifests as the broken line of the I_{output}–I_{input} curve and as a sudden change in the dynamics of the intracavity photon state. When the coupling strength between the exciton and intracavity photon is sufficiently large, a stronger external field is required to disrupt the equilibrium state of the intracavity system, and when L_{cavity} is very large, the population transfer between the exciton and intracavity photon is suppressed due to the small coupling strength between the exciton and intracavity photon. Therefore, a stronger external field is needed to produce a sudden change in the dynamics of the intracavity photon state. From this physical picture, it is not difficult to understand that

the laser threshold varies with L_{cavity}. It is worth noting that there is no direct correspondence between the laser threshold and the steady-state population of the intracavity photon state. This is because the laser threshold is controlled by the short-time excitation of the external field and belongs to the short-time dynamical property; the steady-state population of the intracavity photon state is controlled by the interaction of different components in the total system, which is determined by the long-time dynamical property. Therefore, the combination of the low laser threshold and the large steady-state population of the intracavity photon state may exist. This is indeed reflected in Figure 4. The population dynamics of the ground state, local excited state, and photon state at different cavity lengths are shown in Figures S1–S3, respectively. Of course, when cavity length L_{cavity} is very large (exciton–photon coupling V_{ep} is smaller than intracavity photon leakage rate Γ_P), the steady-state population of the intracavity photon state will indeed decrease monotonically as L_{cavity} increases, as shown in Figure S4. From Figure 3b, we can see that the laser intensity threshold has a linear relationship as the intracavity photon–bath coupling strength increases, and the laser intensity threshold is inversely proportional to the quality of the cavity. When the intracavity photon–bath coupling strength is set to 0.0, the laser intensity threshold is also equal to zero. The results are shown in Figure S7. This indicates that when we change the intracavity photon–bath coupling strength values, we can obtain laser thresholds of any size. On the basis of this linear relationship, we are not limited to the specific values of the laser threshold but focus on the structure–property relationship. It is worth noting that as the intracavity photon leakage rate increases, it does lead to an increase in the initial population of the intracavity photon state and a decrease in the steady-state population of the intracavity photon state, as shown in Figure 5.

Next, we calculate the structure–property relationship between the electronic structure properties of a single molecule and the laser threshold. We investigate the influence of the energy of the S_1 state (ε_e), the molecular transition dipole (μ_{eg}), and the reorganization energy (λ_m) on laser threshold I_{thred}. Here, we set L_{cavity} to 15.0 nm and λ_P to 0.5 meV. All unchanged parameters still use the molecular parameters of BSBCz, as mentioned above. For the calculation of the reorganization energy, we use Debye spectral density $J(\omega) = \frac{2\lambda_m \omega \omega_c}{\omega^2 + \omega_c^2}$ to describe the exciton–phonon coupling. Here, we change reorganization energy λ_m, and characteristic frequency ω_c is set to 1450.0 cm^{-1}.[13,24,39] The calculated results are shown in Figure 6. From the results, we can see that laser threshold I_{thred} monotonically decreases as molecular S_1-state energy ε_e and molecular transition dipole μ_{eg} increase, but reorganization energy λ_m cannot change laser threshold I_{thred}. Molecular S_1-state energy ε_e and molecular transition dipole μ_{eg} are inversely proportional to laser threshold I_{thred}. This is consistent with the experimental results.[40] When molecular S_1-state energy ε_e decreases, the intracavity photons will be quenched faster (shown in Table 2), which leads to the

Table 1. Intracavity Photon Leakage Rates Γ_P and Quality of Cavity Q Values at Different Intracavity Photon–Outside Cavity Bath Coupling Strength λ_P

λ_P (meV)	0.0	0.5	1.0	5.0	10.0	20.0	50.0	100.0	200.0
Γ_P (meV)	0.0	0.1447	0.289	1.447	2.894	5.787	14.47	28.94	57.87
Q	infinity	8542.64	4271.32	854.26	427.13	213.57	85.43	42.71	21.36

Table 2. Intracavity Photon Leakage Rates Γ_P and Quality of Cavity Q Values at Different Intracavity Photon Frequencies ω_P
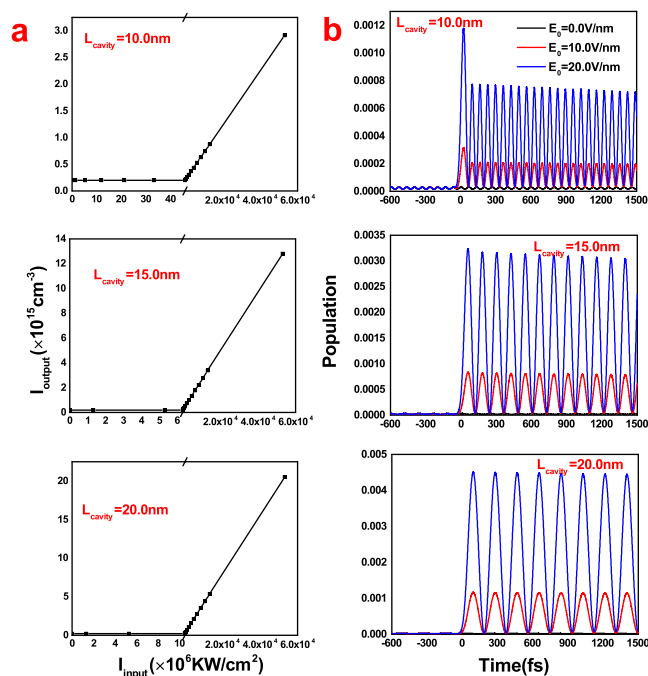
ω_P (eV)	2.0	2.2	2.4	2.6	2.8	3.0
Γ_P (meV)	0.1783	0.1624	0.1490	0.1376	0.1279	0.1190
Q	5607.37	6775.48	8054.84	9445.44	10947.30	12560.40

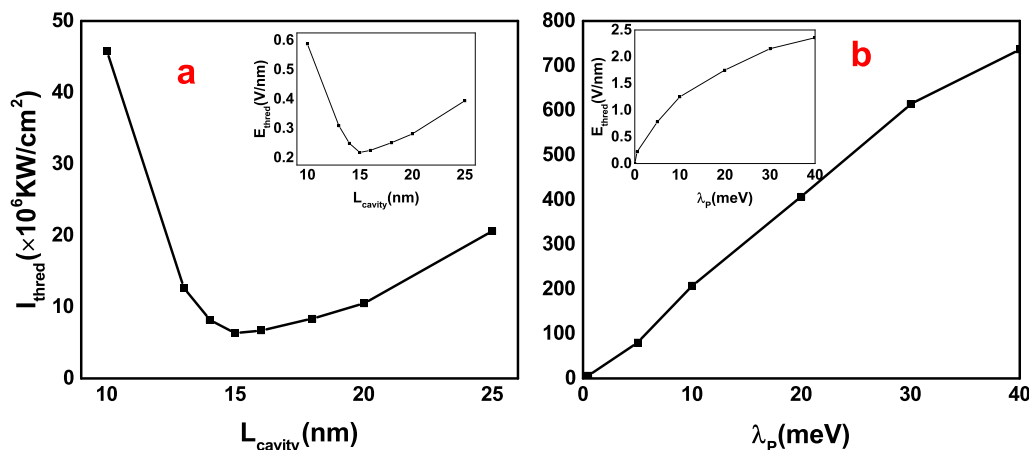**Table 3. Exciton−Photon Couplings V_{ep} at Different Cavity Lengths L_{cavity}**

L_{cavity} (nm)	10.0	13.0	15.0	16.0	18.0	20.0	25.0
V_{ep} (meV)	31.55	21.08	17.18	15.44	12.94	11.16	7.91

increase in laser threshold I_{thred}. The decrease in molecular transition dipole μ_{eg} will weaken the ability of external fields to disrupt the initial steady state of the intracavity system, leading to an increase in laser threshold I_{thred}, although reorganization energy λ_m has almost no effect on laser threshold I_{thred}. However, the increase in reorganization energy λ_m can reduce the steady-state population of the intracavity photon state, which does hinder light amplification in the cavity. The calculated population dynamics of the intracavity photon state is shown in Figure S8. As we know, the Debye spectral density is very suitable for describing the low-frequency vibrational modes of a molecule. When we increase λ_m, the low-frequency vibrational modes are enhanced and the high-frequency modes are almost unaffected. Therefore, the molecular "four-level" energy system is ruined. This is consistent with the conclusion proposed by ref 18. In this work, we cannot consider the influence of the molecular aggregation effect on laser threshold I_{thred}, and we will extend the current work to investigate the influence of the molecular aggregation effect on laser threshold I_{thred} in our future work.

Finally, we investigate the effects of temperature T and external field duration σ on laser threshold I_{thred}, and the calculated results are shown in Figure 7. From the results of the calculation, we can see that temperature T and external field duration σ cannot change laser threshold I_{thred}. From the population dynamics of the intracavity photon state, one can see that the increase in temperature T can accelerate the relaxation of the intracavity system. It is noteworthy that temperature T directly affects the steady-state population of the intracavity photon state, which is a long-time dynamical property, and, the steady-state population of the intracavity

Figure 4. (a) $I_{output}-I_{input}$ curve at different cavity lengths L_{cavity}. (b) Population dynamics of the photon state inside the subsystem that includes one molecule and one photon at different cavity length L_{cavity}.

photon state is controlled by the interaction of different components in the total system. The laser threshold is a short-time dynamical property, which is controlled by the short-time excitation of the external field, and there is no direct correspondence between the laser threshold and the steady-state population of the intracavity photon state. The short-time population dynamics of the intracavity photon state cannot be affected by temperature, as shown in Figure S9. An increase in external field duration σ can decrease the external field strength at $t = 0.0$, thereby reducing the population of the intracavity

Figure 3. Structure−property relationship between (a) cavity length L_{cavity} and laser threshold I_{thred} and (b) intracavity photon−outside cavity bath coupling strength λ_P and laser threshold I_{thred}. The inset shows the structure−property relationship with respect to field strength threshold E_{thred}.

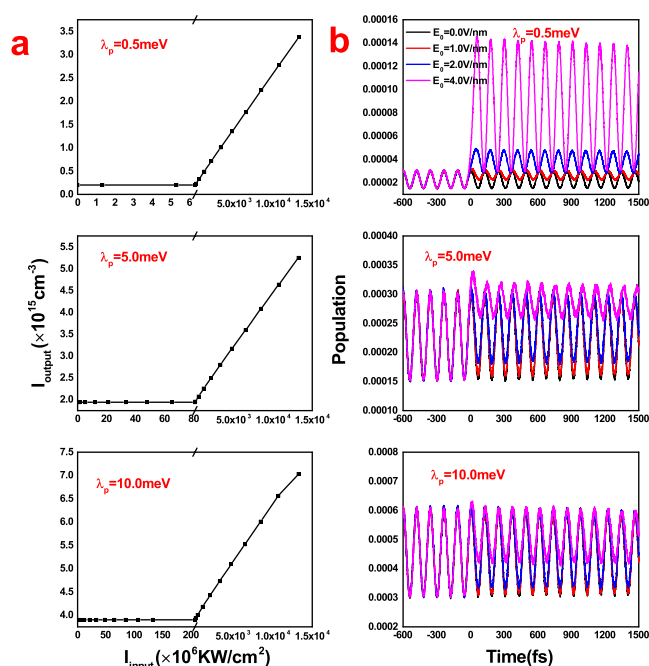**Figure 5.** (a) $I_{\text{output}}-I_{\text{input}}$ curve at different intracavity photon−outside cavity bath coupling strengths λ_{P}. (b) Population dynamics of the photon state inside the subsystem that includes one molecule and one photon at different intracavity photon−outside cavity bath coupling strengths λ_{P}.

Figure 7. Relationship between temperature T and duration σ and laser threshold I_{thred} (left). Population dynamics of the photon state inside the subsystem that includes one molecule and one photon at different temperatures T and durations σ.

photon state. Although the action time of external field $E_{\text{pump}}(t)$ will increase with duration σ, a smaller duration σ is indeed beneficial for increasing the steady-state population of the intracavity photon state. It is worth noting that increasing duration σ does not mean that external field $E_{\text{pump}}(t)$ can exhibit the performance of a continuous wave. When duration σ approaches infinity, external field $E_{\text{pump}}(t)$ has no effect on the intracavity system.

In conclusion, on the basis of the TDWPD method coupled with light−matter interaction, we develop a microscopic quantum dynamic approach to describe the organic lasing phenomena in a dissipative cavity. The extended TDWPD method is applied to investigate the structure−property relationships between the lasing threshold and the intracavity photon−outside cavity bath coupling strength, cavity size, and single-molecule electronic structure properties. The following conclusions are drawn. (i) A microscopic model suitable for
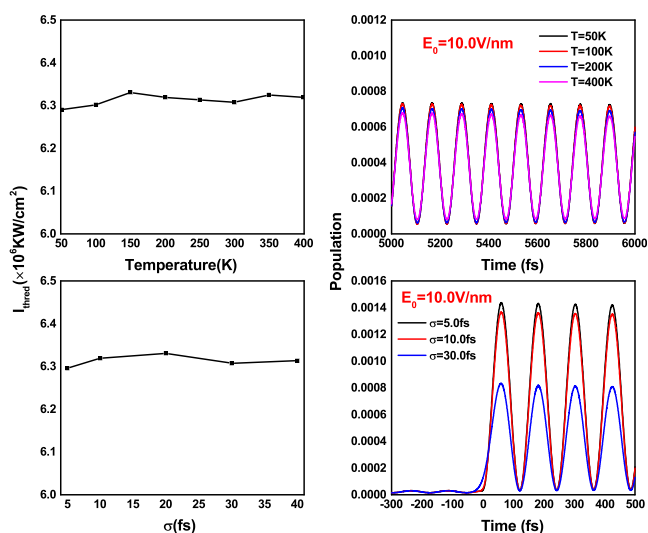
describing the lasing dynamics of an organic molecular system has been constructed, which can be used to describe the structure−property relationships between the laser threshold and cavity parameters and molecular electronic structure parameters. (ii) The microscopic physical picture of an organic laser is proposed. The photons outside the cavity can penetrate the cavity, leading to the thermal equilibrium state in the cavity. Only when the intensity of the external field is sufficient to break the equilibrium state of the intracavity system will the lasing phenomenon happen. (iii) The laser threshold decreases first and then increases as the cavity size increases, and there is an optimal value that can be understood from a physical perspective. The laser threshold increases linearly with the intracavity photon−outside cavity bath coupling strength, exhibiting a monotonically decreasing tendency with an increase in the cavity quality value (Q value), which is consistent with the experimental results. (iv) The reorganization energy cannot change the laser threshold. A larger reorganization energy leads to a decrease in the steady-state population of the intracavity photon state. The energy of the S_1 state and the transition dipole are inversely proportional to the laser threshold, which is consistent with the experimental conclusion. The proposed formalism and structure−property
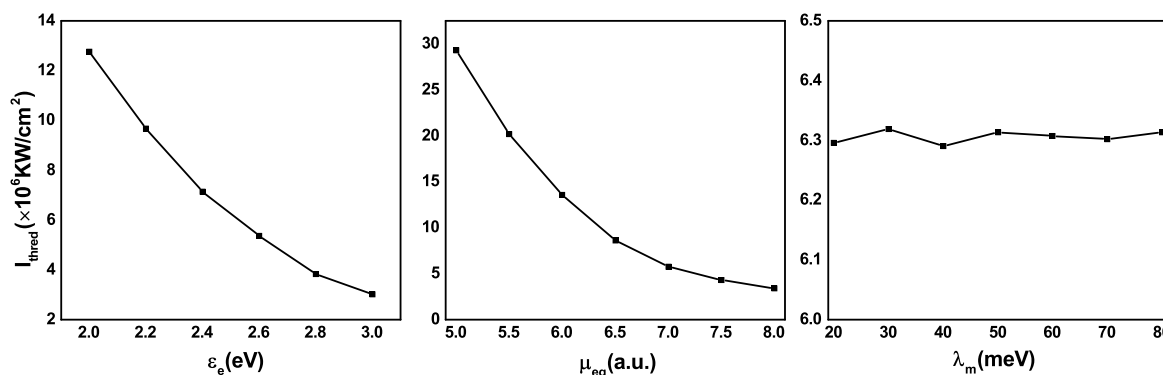

Figure 6. Structure−property relationship between molecular S_1-state energy ε_e, molecular transition dipole μ_{eg}, and reorganization energy λ_m and laser threshold I_{thred}.

relationship are beneficial for understanding the mechanism of organic laser and optimizing the design of organic laser materials.

ASSOCIATED CONTENT

Supporting Information

The Supporting Information is available free of charge at https://pubs.acs.org/doi/10.1021/acs.jpclett.3c02171.

Introduction of the random orientation model; population dynamics of the ground state, local excited state, and photon state inside the subsystem that includes one molecule and one photon at different cavity lengths; $I_{output}-I_{input}$ curve at a cavity length L_{cavity} of 15.0 nm and an intracavity photon−outside cavity bath coupling strength λ_P of 0.0 meV; and population dynamics of the photon state inside the subsystem that includes one molecule and one photon at different reorganization energies λ_m (PDF)

AUTHOR INFORMATION

Corresponding Author

Zhigang Shuai − *School of Science and Engineering, The Chinese University of Hong Kong, Shenzhen, Guangdong 518172, P. R. China;* orcid.org/0000-0003-3867-2331; Email: shuaizhigang@cuhk.edu.cn

Author

Bin Zhang − *MOE Key Laboratory of Organic OptoElectronics and Molecular Engineering, Department of Chemistry, Tsinghua University, Beijing 100084, China;* orcid.org/0000-0002-0170-2923

Complete contact information is available at:
https://pubs.acs.org/10.1021/acs.jpclett.3c02171

Notes

The authors declare no competing financial interest.

ACKNOWLEDGMENTS

REFERENCES

(1) Fichou, D.; Delysse, S.; Nunzi, J. M. First evidence of stimulated emission from a monolithic organic single crystal: α-Octithiophene. *Adv. Mater.* **1997**, *9*, 1178−1181.

(2) Lee, E.; Medvedev, E. S.; Stuchebrukhov, A. A. Effect of quantum modes in biological electron transfer reactions: A useful approximation for the harmonic model with frequency change and Duchinsky rotation. *J. Chem. Phys.* **2000**, *112*, 9015.

(3) Hwang, H.; Rossky, P. J. Electronic Decoherence Induced by Intramolecular Vibrational Motions in a Betaine Dye Molecule. *J. Phys. Chem. B* **2004**, *108*, 6723.

(4) Zhao, Y.; Liang, W. Z.; Nakamura, H. Semiclassical Treatment of Thermally Activated Electron Transfer in the Intermediate to Strong Electronic Coupling Regime under the Fast Dielectric Relaxation. *J. Phys. Chem. A* **2006**, *110*, 8204.

(5) Liang, W. Z.; Zhao, Y.; Sun, J.; Song, J.; Hu, S. L.; Yang, J. L. Electronic Excitation of Polyfluorenes: A Theoretical Study. *J. Phys. Chem. B* **2006**, *110*, 9908−9915.

(6) Samuel, I. D. W.; Turnbull, G. A. Organic semiconductor lasers. *Chem. Rev.* **2007**, *107*, 1272−1295.

(7) Peng, Q.; Yi, Y.; Shuai, Z.; Shao, J. Toward Quantitative Prediction of Molecular Fluorescence Quantum Efficiency: Role of Duschinsky Rotation. *J. Am. Chem. Soc.* **2007**, *129*, 9333−9339.

(8) Sun, J.; Guo, Z. Y.; Liang, W. Z. Harmonic generation of open-ended and capped carbon nanotubes investigated by time-dependent Hartree-Fock theory. *Phys. Rev. B* **2007**, *75*, 195438.

(9) Zhong, X. X.; Zhao, Y. Charge Carrier Dynamics in Phonon-Induced Fluctuation Systems from Time-Dependent Wavepacket Diffusion Approach. *J. Chem. Phys.* **2011**, *135*, 134110.

(10) Chénais, S.; Forget, S. Recent advances in solid-state organic lasers. *Polym. Int.* **2012**, *61*, 390−406.

(11) Zhang, W. W.; Zhong, X. X.; Zhao, Y. Electron Mobilities of n-Type Organic Semiconductors from Time-Dependent Wavepacket Diffusion Method: Pentacenequinone Derivatives. *J. Phys. Chem. A* **2012**, *116*, 11075.

(12) Zhong, X. X.; Zhao, Y. Non-Markovian Stochastic Schrodinger Equation at Finite Temperatures for Charge Carrier Dynamics in Organic Crystals. *J. Chem. Phys.* **2013**, *138*, 014111.

(13) Berkelbach, T. C.; Hybertsen, M. S.; Reichman, D. R. Microscopic Theory of Singlet Exciton Fission. II. Application to Pentacene Dimers and the Role of Superexchange. *J. Chem. Phys.* **2013**, *138*, 114103.

(14) Schneider, C.; Rahimi-Iman, A.; Kim, N. Y.; Fischer, J.; Savenko, I. G.; Amthor, M.; Lermer, M.; Wolf, A.; Worschech, L.; Kulakovskii, V. D.; Shelykh, I. A.; Kamp, M.; Reitzenstein, S.; Forchel, A.; Yamamoto, Y.; Hofling, S. An electrically pumped polariton laser. *Nature* **2013**, *497*, 348−352.

(15) Cui, Q. H.; Zhao, Y. S.; Yao, J. Controlled synthesis of organic nanophotonic materials with specific structures and compositions. *Adv. Mater.* **2014**, *26*, 6852−6870.

(16) Shuai, Z.; Peng, Q. Excited States Structure and Processes: Understanding Organic Light-Emitting Diodes at the Molecular Level. *Phys. Rep.* **2014**, *537*, 123−156.

(17) Han, L.; Ke, Y. L.; Zhong, X. X.; Zhao, Y. Time-Dependent Wavepacket Diffusion Method and Its Applications in Organic Semiconductors. *Int. J. Quantum Chem.* **2015**, *115*, 578−588.

(18) Ma, L.; Wu, Z.; Zhou, G.; Yuan, F.; Yu, Y.; Yao, C.; Ning, S.; Hou, X.; Li, Y.; Wang, S.; Gong, Q. The Molecular Picture of Amplified Spontaneous Emission of Star-Shaped Functionalized-Truxene Derivatives. *J. Mater. Chem. C* **2015**, *3*, 7004−7013.

(19) Kuehne, A. J. C.; Gather, M. C. Organic lasers: recent developments on materials, device geometries, and fabrication techniques. *Chem. Rev.* **2016**, *116*, 12823−12864.

(20) Gierschner, J.; Varghese, S.; Park, S. Y. Organic single crystal lasers: a materials view. *Adv. Opt. Mater.* **2016**, *4*, 348−364.

(21) Ebbesen, T. W. Hybrid Light-Matter States in a Molecular and Material Science Perspective. *Acc. Chem. Res.* **2016**, *49*, 2403−2412.

(22) Frisch, M. J.; Trucks, G. W.; Schlegel, H. B.; Scuseria, G. E.; Robb, M. A.; Cheeseman, J. R.; Scalmani, G.; Barone, V.; Petersson, G. A.; Nakatsuji, H.; et al., *Gaussian 16*, rev. B.01; Gaussian, Inc.: Wallingford, CT, 2016.

(23) Sandanayaka, A. S. D.; Yoshida, K.; Inoue, M.; Qin, C. J.; Goushi, K.; Ribierre, J. C.; Matsushima, T.; Adachi, C. Quasi-Continuous-Wave Organic Thin-Film Distributed Feedback Laser. *Adv. Opt. Mater.* **2016**, *4*, 834−839.

(24) Zang, H.; Zhao, Y.; Liang, W. Z. Quantum Interference in Singlet Fission: J- and H-Aggregate Behavior. *J. Phys. Chem. Lett.* **2017**, *8*, 5105−5112.

(25) Zhu, Z. Y.; Zang, H.; Zhao, Y.; Liang, W. Z. Charge Carrier Mobilities and Singlet Fission Dynamics in Thienoquinoidal Compounds. *J. Phys. Chem. C* **2017**, *121*, 22587−22596.

(26) Shuai, Z.; Peng, Q. Organic Light-Emitting Diodes: Theoretical Understanding of Highly Efficient Materials and Development of Computational Methodology. *Nat. Sci. Rev.* **2017**, *4*, 224−239.

(27) Sandanayaka, A. S. D.; Matsushima, T.; Bencheikh, F.; Terakawa, S.; Potscavage, W. J., Jr.; Qin, C. J.; Fujihara, T.; Goushi, K.; Ribierre, J. C.; Adachi, C. Indication of current-injection lasing from an organic semiconductor. *Appl. Phys. Express* **2019**, *12*, 061010.

(28) Wang, Y.; Peng, Q.; Ou, Q.; Lin, S.; Shuai, Z. A Novel Molecular Descriptor for Highly Efficient ($\Phi_{TADF} > 90\%$) Transition Metal TADF Au(iii) Complexes. *J. Mater. Chem. A* **2020**, *8*, 18721−18725.

(29) Wang, S. W.; Scholes, G. D.; Hsu, L. Y. Coherent-to-Incoherent Transition of Molecular Fluorescence Controlled by Surface Plasmon Polaritons. *J. Phys. Chem. Lett.* **2020**, *11*, 5948−5955.

(30) Jiang, Y.; Liu, Y. Y.; Liu, X.; Lin, H.; Gao, K.; Lai, W. Y.; Huang, W. Organic solid-state lasers: a materials view and future development. *Chem. Soc. Rev.* **2020**, *49*, 5885−5944.

(31) Shuai, Z. Thermal Vibration Correlation Function Formalism for Molecular Excited State Decay Rates. *Chin. J. Chem.* **2020**, *38*, 1223−1232.

(32) Ren, J. H.; Liao, Q.; Huang, H.; Li, Y.; Gao, T. G.; Ma, X. K.; Schumacher, S.; Yao, J. N.; Bai, S. M.; Fu, H. B. Efficient Bosonic Condensation of Exciton Polaritons in an H-Aggregate Organic Single-Crystal Microcavity. *Nano Lett.* **2020**, *20*, 7550−7557.

(33) Sun, J.; Ding, Z. L.; Yu, Y. Q.; Liang, W. Z. Plasmon-enhanced high order harmonic generation of open-ended finite-sized carbon nanotubes: The effects of incident field's intensity and frequency and the interference between the incident and scattered fields. *J. Chem. Phys.* **2020**, *152*, 224708.

(34) Ou, Q.; Peng, Q.; Shuai, Z. Computational screen-out strategy for electrically pumped organic laser materials. *Nat. Commun.* **2020**, *11*, 4485.

(35) Ou, Q.; Shao, Y.; Shuai, Z. Enhanced Reverse Intersystem Crossing Promoted by Triplet Exciton-Photon Coupling. *J. Am. Chem. Soc.* **2021**, *143*, 17786−17792.

(36) Wang, S. W.; Chuang, Y. T.; Hsu, L. Y. Simple but accurate estimation of light-matter coupling strength and optical loss for a molecular emitter coupled with photonic modes. *J. Chem. Phys.* **2021**, *155*, 134117.

(37) Lin, S.; Ou, Q.; Wang, Y.; Peng, Q.; Shuai, Z. Aggregation-Enhanced Thermally Activated Delayed Fluorescence Efficiency for Two-Coordinate Carbene-Metal-Amide Complexes: A QM/MM Study. *J. Phys. Chem. Lett.* **2021**, *12*, 2944−2953.

(38) Jiang, Z. J.; Ren, A.; Yan, Y. L.; Yao, J. N.; Zhao, Y. S. Exciton-Polaritons and Their Bose−Einstein Condensates in Organic Semiconductor Microcavities. *Adv. Mater.* **2022**, *34*, 2106095.

(39) Zhang, B.; Zhao, Y.; Liang, W. Z. Joint Effects of Exciton-Exciton and Exciton-Photon Couplings on the Singlet Fission Dynamics in Organic Aggregates. *J. Phys. Chem. C* **2021**, *125*, 1654−1664.

(40) Oyama, Y.; Mamada, M.; Kondo, A.; Adachi, C. Advantages of naphthalene as a building block for organic solid state laser dyes: smaller energy gaps and enhanced stability. *J. Mater. Chem. C* **2021**, *9*, 4112.

(41) Lin, S. Y.; Ou, Q.; Shuai, Z. Computational Selection of Thermally Activated Delayed Fluorescence (TADF) Molecules with Promising Electrically Pumped Lasing Property. *ACS Materials Lett.* **2022**, *4*, 487−496.

(42) Yazdani, S. A.; Mikaeili, A.; Bencheikh, F.; Adachi, C. Impact of excitonic and photonic loss mechanisms on the threshold and slope efficiency of organic semiconductor lasers. *Jpn. J. Appl. Phys.* **2022**, *61*, 074003.

(43) Abe, A.; Goushi, K.; Sandanayaka, A. S. D.; Komatsu, R.; Fujihara, T.; Mamada, M.; Adachi, C. Numerical Study of Triplet Dynamics in Organic Semiconductors Aimed for the Active Utilization of Triplets by TADF under Continuous-Wave Lasing. *J. Phys. Chem. Lett.* **2022**, *13*, 1323−1329.

(44) Lindoy, L. P.; Mandal, A.; Reichman, D. R. Quantum dynamical effects of vibrational strong coupling in chemical reactivity. *Nat. Commun.* **2023**, *14*, 2733.

(45) Jiang, T.; Ren, J. J.; Shuai, Z. G. Unified Definition of Exciton Coherence Length for Exciton-Phonon Coupled Molecular Aggregates. *J. Phys. Chem. Lett.* **2023**, *14*, 4541−4547.

(46) Wang, Y.; Ren, J.; Shuai, Z. Minimizing non-radiative decay in molecular aggregates through control of excitonic coupling. *Nat. Commun.* **2023**, *14*, 5056.

(47) Liu, R.; Ge, Y.; Wang, D.; Shuai, Z. Understanding the Temperature Dependence of the Seebeck Coefficient from First-Principles Band Structure Calculations for Organic Thermoelectric. *CCS Chem.* **2021**, *3* (4), 1477.